Numerical and experimental investigation on the cavitating flow in a cascade of hydrofoils

R. Lohrberg, Darmstadt Stoffel, Regiane . Fortes Patella, Olivier Coutier-Delghosa, Jean-Luc Reboud

Numerical and experimental investigations on the cavitating flow in a cascade of hydrofoils

H. Lohrberg, B. Stoffel, R. Fortes-Patella, O. Coutier-Delgosha, J.L. Reboud

Abstract The cavitating flow in a cascade of three hydrofoils was investigated by experimental means and numerical simulation. Experiments on the 2D-hydrofoils cascade were carried out at Darmstadt University of Technology in a rectangular test section of a cavitation tunnel. A numerical model developed at LEGI (Grenoble) to describe the unsteady behaviour of cavitation, including the shedding of vapour structures, was applied to the hydrofoils cascade geometry. Results of both experimental and numerical studies show a strong interaction between the cavities of each flow channel besides the typical self-oscillation of cloud cavitation. A detailed comparison of the results allows an interpretation of the interaction mechanisms to be proposed.

List of symbols

C_p	pressure coefficient=$(P-P_{upstream})/(1/2\rho_l V_{ref}^2)$
f	frequency, Hz
L_{cav}	cavity length, m
L_{ref}	reference length=chord of the foil=5 cm, m
V_{ref}	reference velocity=inlet flow velocity, m/s
P	static pressure, Pa
P_{ref}	reference pressure=inlet static pressure, Pa
P_v	vapour pressure, Pa
St	Strouhal number=fL_{cav}/V_{ref}
T_{ref}	reference time=L_{ref}/V_{ref}, s
α	angle of velocity vector
σ	cavitation number=$(P_{ref}-P_v)/(1/2\rho_l V_{ref}^2)$
ρ_l	liquid density, kg/m^3

H. Lohrberg (✉), B. Stoffel
Chair of Turbomachinery and Fluid Power,
Darmstadt University of Technology,
Magdalenenstr. 4, 64289 Darmstadt, Germany
E-mail: lohrberg@tfa.tu-darmstadt.de

R. Fortes-Patella, O. Coutier-Delgosha
Laboratoire des Ecoulements Géophysiques et Industriels,
LEGI-ENSHM-INPG, BP 53-38041,
Grenoble Cédex 09, France

J.L. Reboud
LTDS/ENISE, 58 rue Jean Parot,
42023 Saint Etienne Cédex 2, France

This work is part of a European exchange programme PROCOPE with the research teams of Grenoble and Darmstadt as members. The numerical model has been developed with the support of the French space agency CNES.

1 Introduction

In the scope of the European Research Program PROCOPE, researchers of the LEGI (Laboratoire des Ecoulements Géophysiques et Industriels de Grenoble) and of the Chair of Turbomachinery and Fluid Power at Darmstadt University of Technology (TUD) work together in order to improve the understanding of the unsteady behaviour of cavitating flows and the related erosive aggressiveness. In this context, experimental investigation and numerical modelling of cavitating flows around a 2D hydrofoil with a semicircular leading edge were performed. Previous results concerning the self-oscillating behaviour of cloud cavitation were presented by Hofmann et al. (1999), and the stabilising effect of a small obstacle modifying the foil suction side has been more particularly studied. In the present paper, the cavitating flow in a cascade of three hydrofoils was investigated by experimental means and numerical simulation.

Experiments on the 2D-hydrofoils cascade were carried out at TUD in a rectangular test section of a cavitation tunnel. Transient wall pressure signals were measured, treated to evaluate the dominant frequencies and used to perform conditional sampling of images of the cavitating flow. Images of the cavitating flow were taken synchronously with the pressure transients to provide further information about the cavitation dynamics.

Numerical models of unsteady cavitating flows using single fluid approaches have been developed in recent years. In such models, the same velocity is assumed for liquid and vapour phases in the two-phase zones. Vaporisation and condensation of the fluid are managed using a barotropic state law, a mass transfer equation or a bubble dynamic model. Besides applications of different models to quasi-steady cavitating flow, some studies focused on unsteady cloud cavitation phenomena in Venturi-type ducts (Delannoy and Kueny 1990; Reboud et al 1998), around hydrofoils in cavitation tunnels (Kubota et al. 1992; Reboud and Delannoy 1994; Song and He 1998; Sauer and Schnerr 2000) or in centrifugal pumps (Hofmann et al. 2001). Numerical simulation of the stabilising effect of a small obstacle placed in the cavitation sheet area (Hofmann et al. 1999) shows the ability of such a model to catch localised hydrodynamic effects. Recent extension to blade cascades representative of inducer geometries (Coutier-Delgosha et al. 2000) allows instabilities due to the presence of sheet cavitation on the different blades to be predicted, showing a reliable agreement with experimental observations (Joussellin et al. 2001).

In the present paper, the numerical model, developed at LEGI (Grenoble) to describe the unsteady behaviour of cavitation including the shedding of vapour structures, was applied to hydrofoil cascade geometry. Comparisons of experimental and numerical results are performed to analyse the interaction between the cavitating flows in the different channels.

2
Experimental set-up

The object of the investigations was a cascade of three hydrofoils, located in a test section with a rectangular cross section of 30×100 mm (Fig. 1). The hydrofoils can be adjusted to different angles of attack in a range of ±10° according to different flow rates in a centrifugal pump. The flow can be illuminated and observed through a lateral window. Illumination was done with a stroboscopic light source, and images were taken with a CCD camera (PCO sensicam). A piezoresistive pressure transducer (Kulite XTM-190 M) with a frequency range up to 125 kHz was also mounted in the window. The membrane was connected to the flow by a small, short opening. The geometry of the hydrofoils and sensor position are shown in Fig. 1b. The sensor was mounted above profile 1, the positions above profiles 2 and 3 were additionally used for post-processing of the numerical results. The test section was part of a closed hydraulic loop. Flow rate and static pressure could be varied in order to achieve different cavitation conditions. In the case presented hereafter, the hydrofoils were held at a 5° angle of attack, and the inlet velocity V_{ref} was equal to 14 m/s.

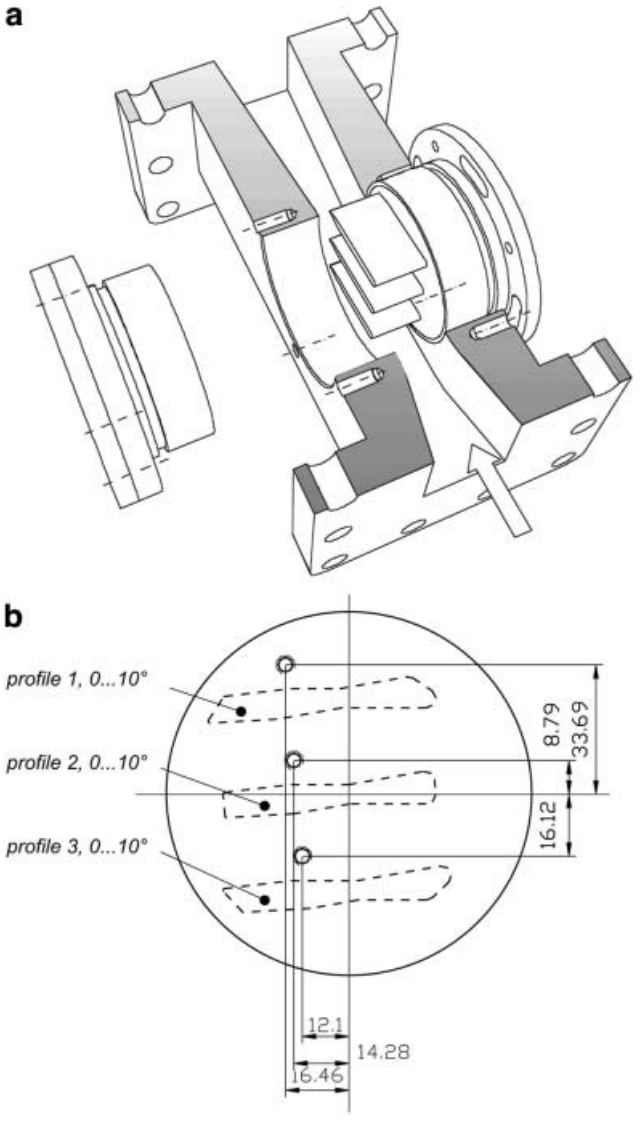

Fig. 1a, b. Hydrofoils cascade geometry: **a** *cut through* the test section (pressure transducers are not shown); **b** *side view* of the window with one sensor (*upper channel*) and three post-processing positions

Image illumination and acquisition and pressure signal recording were both triggered by a personal computer. Signals were sampled with 100 kHz and stored in a transient recorder. Storing started with 50% pre-trigger, thus the image was taken in the middle of the measurement. Images and measurements were read out and stored on the personal computer. Every image was then related to a part of the pressure signal. Unfortunately, parts of the black coating of the channel wall detached during image acquisition, leaving some bright stains around the hydrofoils.

3
Signal treatment

Power density spectra of the pressure signals showed two dominant frequencies for each signal. To extract those frequencies from the very noisy pressure signal, a more careful method was applied to the records.

First the signals were split offline at 100 Hz into high- and low-frequency parts by high- and low-pass filtering respectively. The auto-correlation function was then calculated from both parts. The function of a fully periodic signal would show several peaks, each with a maximum of one. The first is located at zero shifting, the others at positive and negative multiples of cycle duration. Due to the frequency variation of a real signal, these peaks do not have a maximum of one. If the variation is seen as a phase difference between successive periods, the maximum value of the first peak next to the centre is the cosine of this phase difference. The more remote peaks decline exponentially with their distance from the centre. The frequency variation can therefore be calculated from the peak value at cycle duration. Both the frequencies and their variation are shown as functions of the cavitation number σ in Fig. 2.

In contrast to frequency estimation by Fourier transformation, this process delivers a unique fluctuation frequency even of very noisy signals. Furthermore, it is possible to directly derive a frequency instability. The use of this information is described below. In power density spectra, such an unstableness appears as a broadening of the amplitude peak, which is hardly quantifiable.

The higher frequencies correspond to the cavitation self-oscillation behaviour characterised by a Strouhal number between 0.2 and 0.3. The lower frequency was presumed to be related to a coupling of the cavitation on the three hydrofoils. To verify this presumption, images were associated with the phase angle of the low-frequency fluctuation.

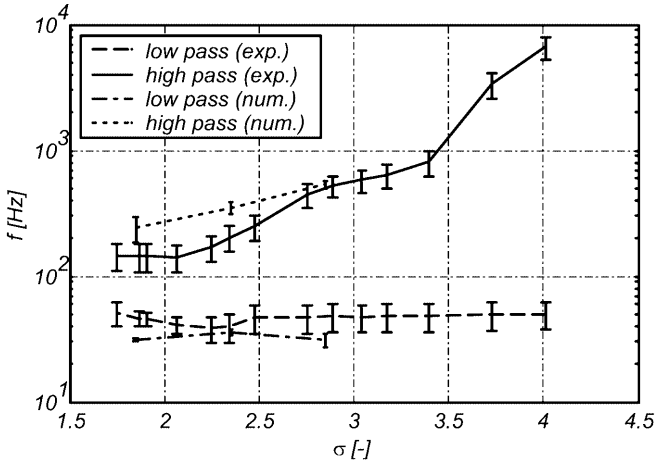

Fig. 2. Main frequency of the low- and high-pass filtered pressure signal as a function of the cavitation number σ, V_{ref}=14 m/s

This fluctuation was extracted by filtering the original signal. The filter design is based on the auto-correlation function of the signal. The mean cycle frequency plus/minus the frequency variation are taken as the edge frequencies of a band-pass filter. Filtering was carried out by Fourier transformation, deletion of the parts with frequencies outside the band and inverse Fourier transformation. This added no delay to the signal.

After filtering, the signals were undertaken to a Hilbert transformation. This transformation adds an imaginary part to the signal by shifting the Fourier coefficients by an angle of $\pi/2$ and performing the inverse Fourier transformation. The phase information can be extracted from the complex signal (Fig. 3). The non-consecutively acquired images can then be sorted into phase angle consecutive order.

With the phase information available for every image, two further treatments could be used to explain the cavitation behaviour and to compare the experimental and the numerical results respectively.

First, the images were put together to an exemplary sequence of one cavitation cycle (Fig. 4). The cycle was

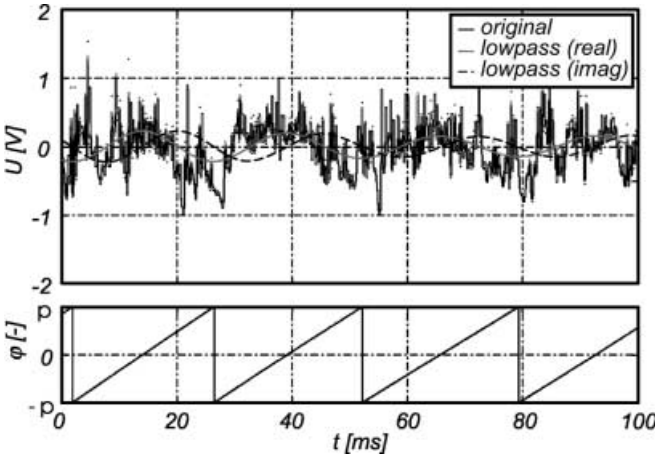

Fig. 3. Raw pressure signal, low-pass filtered and Hilbert transformed signal, phase angle

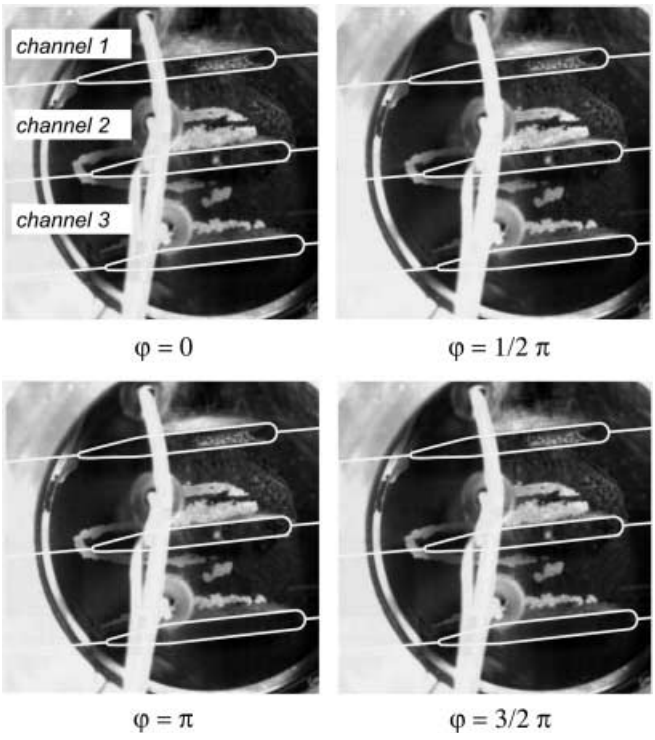

Fig. 4. Exemplary frames from a sequence of phase angle averaged images, α=5°, σ=1.9, V_{ref}=14 m/s

divided into 25 steps. On the basis of the phase angle, each image was assigned to one step. With a total image number of 1,000, each step includes about forty images. These images were averaged by a special algorithm in order to let the resulting image appear like a real one-shot cavitation image. This approach makes the subsequent interpretation of the sequence easier. A wavelet transformation was applied using sigmoid wavelets. The wavelet coefficients were then averaged separately by absolute value and sign, thus keeping the image signals energy in every wavelet form. The inverse transformation was applied to the averaged coefficients.

The second treatment extracted the mean brightness of three regions of interest (ROI), each related to one channel of the cascade. As the vapour appears bright in the image, the mean brightness is a measure of the vapour volume even if the relation between both is not quantitatively known. The ROI mean grey values are normalised by time-averaged value and standard deviation. The first harmonic amplitude of the brightness is calculated. The harmonic functions of each channel are shown in Fig. 5. The amount of the signals energy of the brightness that is stored in the first harmonic (value *e* in the legend) is only about 15%. That means that only a small part of the vapour variation is related to the low fluctuation cycle. The larger part is related to cloud shedding and noise.

4 Numerical model

To model and to analyse the unsteady behaviour of the cavitating flow in the tested hydrofoil cascade, the unsteady cavitating flow model developed at LEGI (Grenoble)

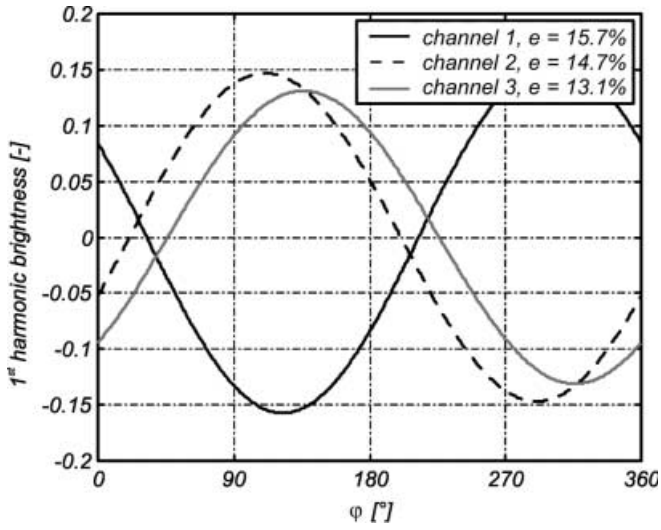

Fig. 5. First harmonic function of the brightness of each channel

(Delannoy and Kueny 1990; Reboud and Delannoy 1994; Reboud et al. 1998) was applied.

The theoretical and numerical model was developed to describe the unsteady behaviour of cavitation, including vapour cloud shedding. In that model, the liquid–vapour two-phase flow is described by a homogeneous flow model with a no-slip condition between liquid and vapour phases. The liquid–vapour mixture, with a void ratio α, is considered as a homogeneous medium and described as a single fluid whose varying specific mass is $\rho=\alpha\rho_v+(1-\alpha)\rho_l$. A simple description of the vaporisation and condensation phenomena is proposed by introducing an empirical barotropic state law $\rho(p)$ for the mixture. A smooth law was chosen, ρ rapidly varying between liquid density ρ_l and vapour density ρ_v when the local static pressure P is around the vapour pressure P_v. The law is characterised by its maximum slope at $P=P_v$, which is related to the minimum speed of sound A_{min} in the two-phase homogeneous medium. A_{min} is the only adjustable parameter of the model, fixed in the present study as in the previous one (Hofmann et al. 1999) at 10% of inlet velocity V_{ref}.

Reynolds-averaged Navier–Stokes equations are solved in the case of this single fluid with variable density. A finite volume spatial discretisation is applied in curvilinear orthogonal coordinates on a staggered mesh.

An iterative resolution based on the SIMPLE algorithm was developed to deal with quasi-incompressible flow ($\alpha=0$ and $\alpha=1$) and highly compressible flow ($0<\alpha<1$) (Delannoy and Kueny 1990). The liquid–vapour interfaces are described by high gradients of the mixture density ρ, which was made possible by using a conservative approach and the HLPA non-oscillatory second-order MUSCL scheme (Zhu 1991). To solve the time-dependent elliptic problem, a first-order fully implicit method is used. Turbulent flows are calculated by solving the Reynolds equations using a k–ϵ RNG turbulence model with standard laws of the wall.

The mass flow rate is imposed constant as an upstream boundary condition. The transient static pressure, imposed as a downstream boundary condition, is slowly decreased from a high value, leading to steady non-cavitating conditions, down to the value required to assure the expected cavitation number σ. Phase change then occurs spontaneously in the regions where the pressure decreases close to the vapour pressure P_v. Because the experimental value of σ is based on an upstream pressure measurement as reference pressure, the losses generated in the cavitation tunnel by viscous and unsteady effects have to be taken into account in the calculation to compare a posteriori the experimental and numerical cavitation numbers.

The model was previously tested in Venturi-type ducts (Reboud et al. 1998) and on single hydrofoil geometries (Reboud and Delannoy 1994; Hofmann et al. 1999). Empirical modification of turbulence dissipative terms in the two-phase regions was proposed, to enhance the simulation of the unsteady behaviour of cavitation observed experimentally: turbulent viscosity in the pure liquid phase remains provided by the classical k–ϵ RNG model, while stronger shear flows are allowed in the two-phase regions by arbitrary reduction of the turbulence model constant C_μ (multiplication by a function $f(\rho)$, equal to 1 for $\rho=\rho_l$ and rapidly decreasing towards ρ_v/ρ_l when $\rho<\rho_l$; Reboud et al. 1998). Eects on unsteady cavitation modelling of other modifications of standard turbulence models have been investigated recently and are reported in (Coutier-Delgosha et al. 2001).

5
Simulation of the unsteady cavitating flow in the cascade

In the case presented below, the static pressure is decreased down to the experimental value $\sigma=1.95$. Vapour structures, characterised in the model by small values of the density ρ, are generated along the suction side of the foils from the leading edge. After the initial transient, a special unsteady behaviour is observed (Fig. 6):

- On the upper foil suction side, typical cloud cavitation behaviour takes place. However, the size and shedding period of the cavitation structures show strong variations between the successive cycles.
- On the two other foils, the cavities appear as almost stable sheets attached to the blades, but with large amplitude and low-frequency fluctuations of length.

The difference between the cavitation behaviour in channel 1 and the others is associated with the larger flow angle of attack observed in front of the upper hydrofoil. This effect is due to the presence of the upper wall. The divergence angle between the wall and the foil suction side, associated with the trailing edge condition, increases the flow rate passing over the foil. An opposite effect occurs between the third foil and the lower wall. With the larger angle of attack, typical unsteady cloud cavitation takes place, while stable sheet cavities with low relative thickness develop on the two other foils (channels 2 and 3). It can be seen in Fig. 6, that the fluctuations of the cavitation structures (i.e. cloud cavitation in channel 1 and attached cavitation sheets in channels 2 and 3) appear with completely opposite phases. Disappearance of the cavitation structures in the upper channel corresponds to a

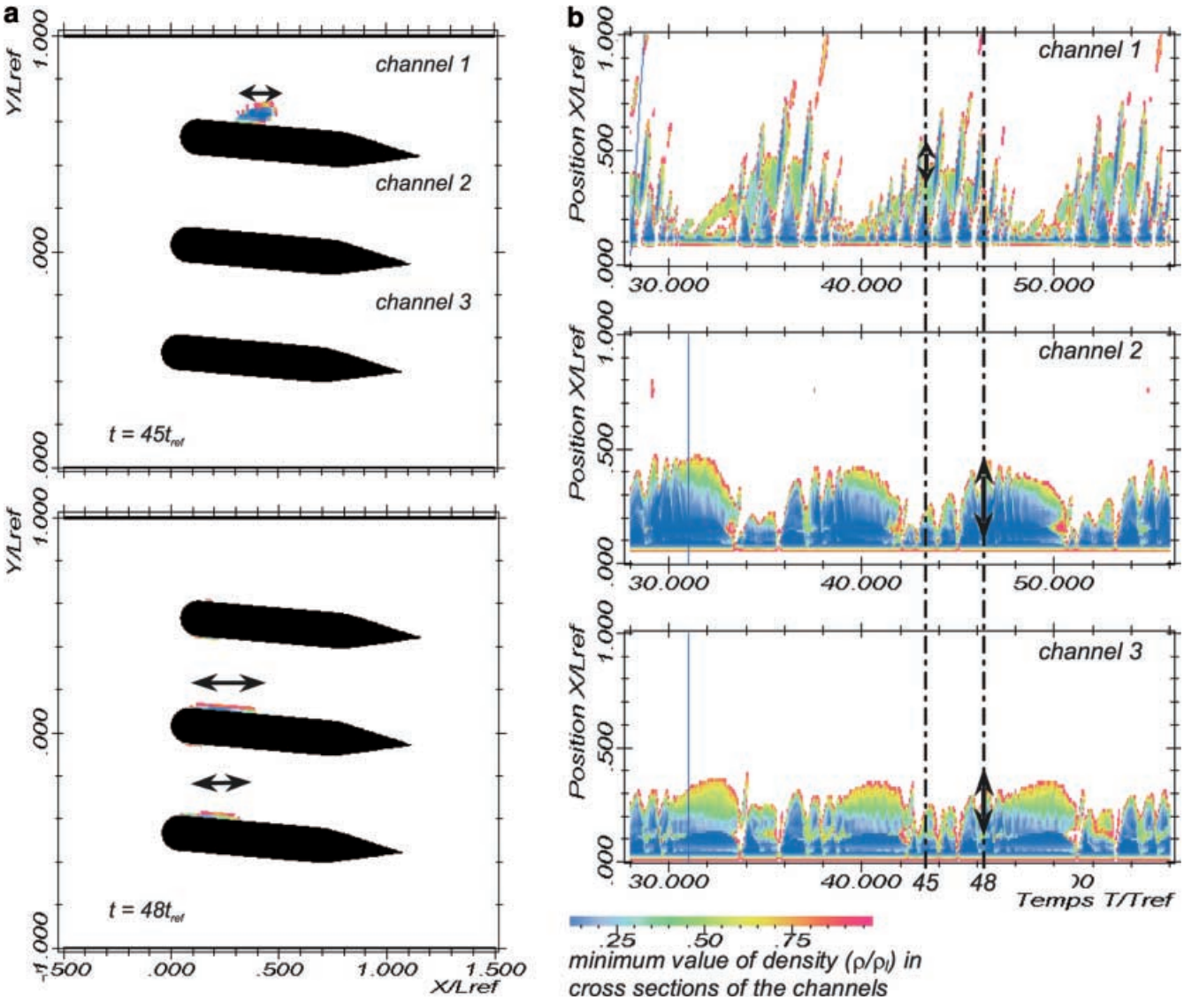

Fig. 6. **a** Time evolution of the cavitation structures on the three hydrofoils (V_{ref}=14 m/s, σ=1.95): density field at t=160 and 172 ms (45 and 48T_{ref}, T_{ref}=L_{ref}/V_{ref}=3.6 ms). **b** Time evolution of the cavitation structures: size of the cavitation structures in the channels

maximum development of the cavitation sheets on the two other foils, and vice versa.

To evaluate the characteristic frequencies of the cavitating flow, the pressure signals obtained by numerical calculations were analysed with the same treatment used in the experimental study (Sect. 3). Figure 7a illustrates the time evolution of numerical pressure signal at the location of the three transducers. Figure 7b presents the auto-correlation function calculated for high-pass and low-pass filtered pressure signals.

From power density spectra, the lowest characteristic frequency obtained equals 31.42±0.98 Hz.

The frequency of the cloud shedding process in the upper channel can also be estimated by the treatment: a frequency of 262±35 Hz is clearly obtained from the signals corresponding to channels 2 and 3. The frequency content of the signal of channel 1 is much more complex, as can be seen from the auto-correlation function (Fig. 7b) and many peaks are observed in the spectra between 160 and 500 Hz.

Based on the corresponding mean attached cavity length (~0.3L_{ref}~1.5 cm), the inlet velocity (V_{ref}=14 m/s) and a frequency of 262 Hz, the Strouhal number is found to be about 0.28. These values present an order of magnitude in good agreement with the experimental measurements obtained from Fig. 2 at σ=1.95 (respectively about 40–50 Hz and 110–180 Hz).

A zoom of transient pressure coefficient distributions corresponding to the locations of the three transducers (Fig. 1) is given in Fig. 8a, while two pressure fields are given at two different times of the low-frequency cycle (Fig. 8b). Larger development of cloud cavitation in channel 1 is associated with high-pressure fluctuations. The amplitude is higher in the first channel, because the travelling clouds pass the point corresponding to the transducer location, but pressure fluctuations can also be

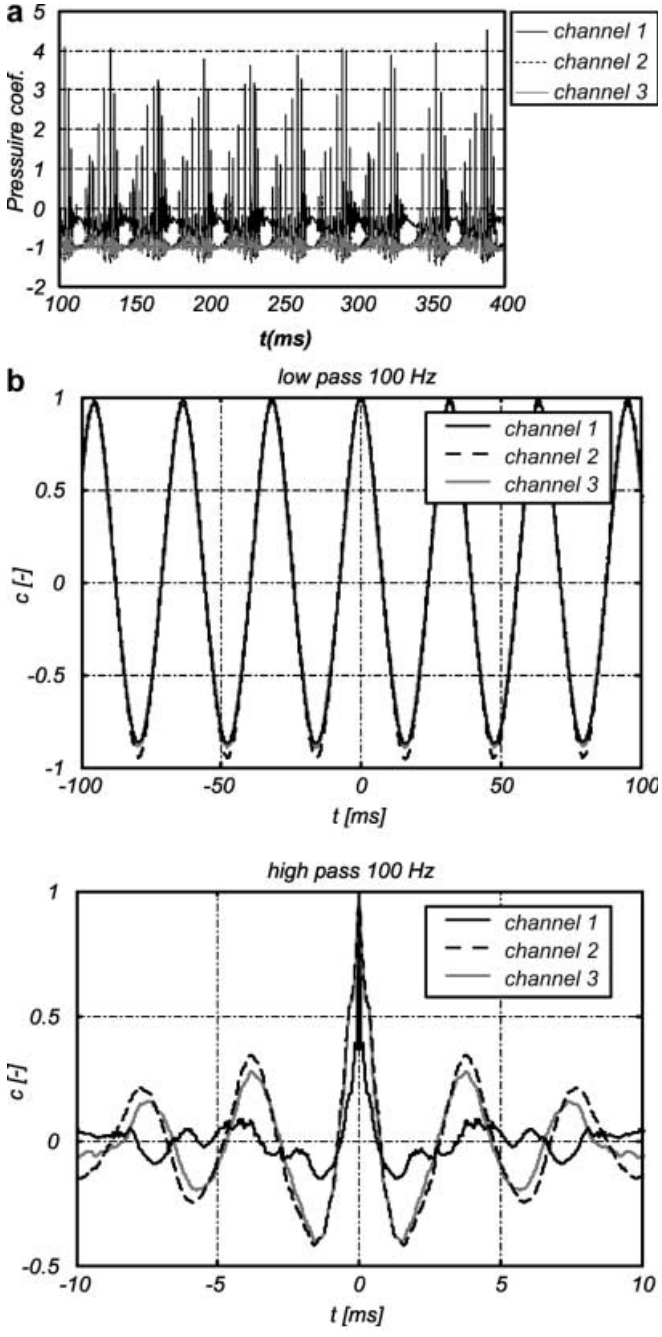

Fig. 7. **a** Time evolution of numerical pressure signal corresponding to the three post-processing positions (σ=1.95). **b** Auto-correlation function calculated for low-pass (*top*) and high-pass filtered pressure signals (*bottom*) for the three transducers (σ=1.95)

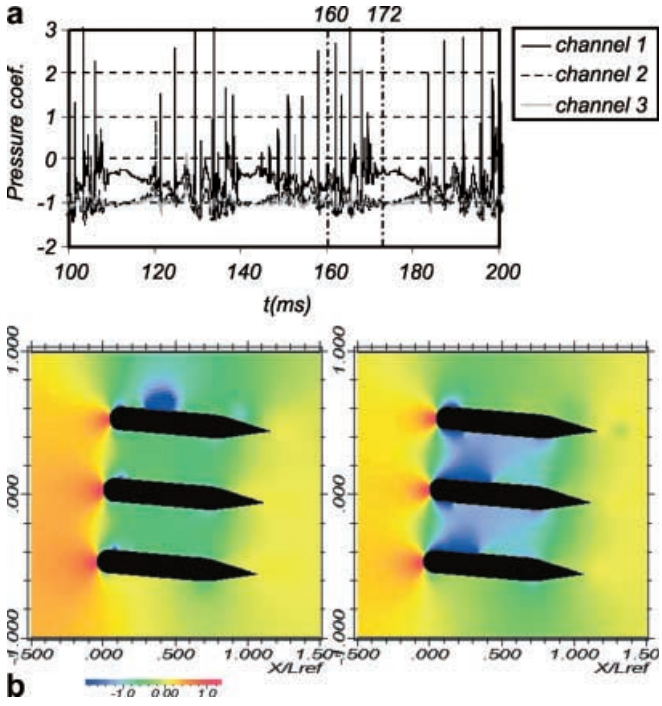

Fig. 8. **a** Numerical pressure signal at the location of the three transducers. **b** Pressure coefficient distribution, t=160 (*left*), t=172 ms (*right*)

clearly noticed in the two other channels. On the contrary, the periods during which cavitation is more developed as stable sheets on the two other foils show a complete stabilisation of the pressure signal.

Figure 9a shows the time variation of the vapour volume computed in the three channels. The treatment developed in the experimental study was applied on the numerical result to evaluate the first harmonic amplitude of the vapour volume calculated for each channel (Fig. 9b).

The result obtained is similar to the experimental one drawn in Fig. 5. The opposite phase behaviour between channel 1 and the two others is clearly visible. A small phase shift between channels 2 and 3 may be noticed too. Nevertheless, the volume of vapour obtained by numerical calculation is characterised by a phase delay to the pressure signal in channel 1 that is different from the one observed in the experiments. The difference between calculations and experiments could be related to the position of the transducer. Indeed, the sensor geometric position is the same in numerical and experimental cases, but the position with regard to the cavitation structures is slightly different for each case (since the cavity length is underestimated by the numerical simulations).

The amplitude of the numerical signal energies estimated by fit of the first harmonic is higher than the ones obtained from the experimental results owing to of the better precision of the numerical calculations.

Despite the observed different cavitation behaviour in each channel, the order of magnitude of the vapour volume predicted by the simulation remains the same in the three channels.

To investigate the reason for the coupling at low frequency between the cavitating flows in the different channels, the time evolution of the local flow angle in front of the upper foil was first drawn (Fig. 10a). As explained before, the occurrence of large cloud cavitation in channel 1 corresponds to the increase in the incident flow angle. In contrast, periods with stable cavitation sheets on the second and third foils correspond to a small flow angle. Longitudinal velocity near the trailing edge, in the boundary layer of the suction side of the upper foil, is drawn Fig. 10b with respect to time. It shows that periods of developed cloud cavitation are followed by the passage

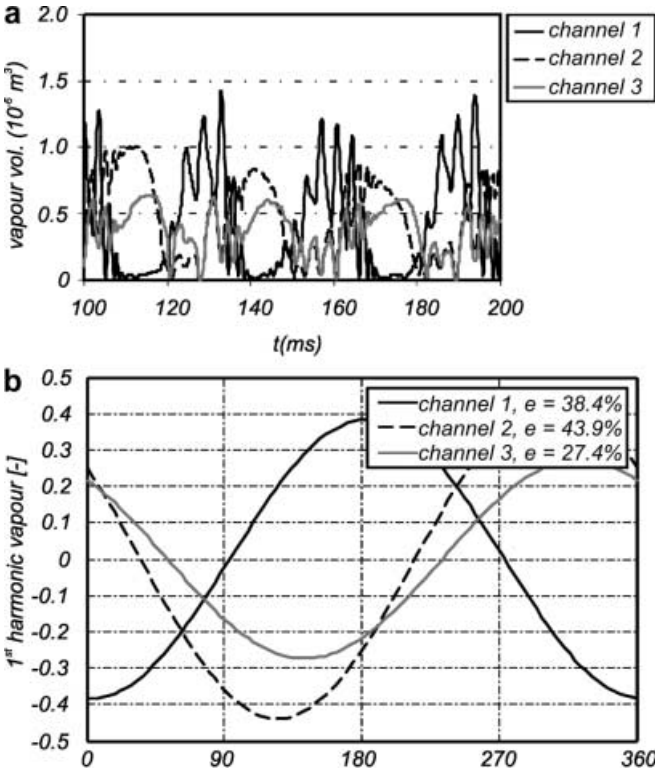

Fig. 9. **a** Time evolution of the vapour volume in the three channels. **b** First harmonic amplitude of the vapour volume calculated for each channel

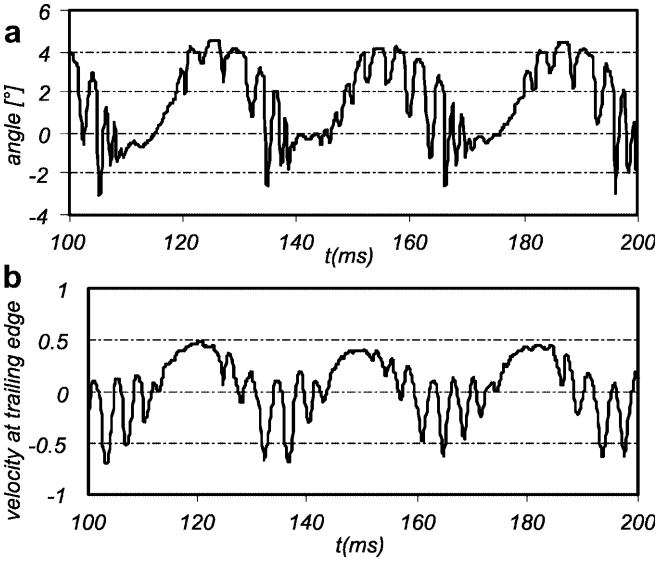

Fig. 10. **a** Angle of velocity vector, 5% upstream of the upper foil leading edge. **b** Longitudinal velocity near the upper foil trailing edge (suction side)

of travelling vortices at the foil trailing edge, with negative longitudinal velocity. The interactions between these travelling flow structures and the foil trailing edge seem to be at the origin of the decrease in the flow angle in front of the foil.

Another illustration of this phenomenon is given in Fig. 11, where the flow vorticity is drawn at different stages

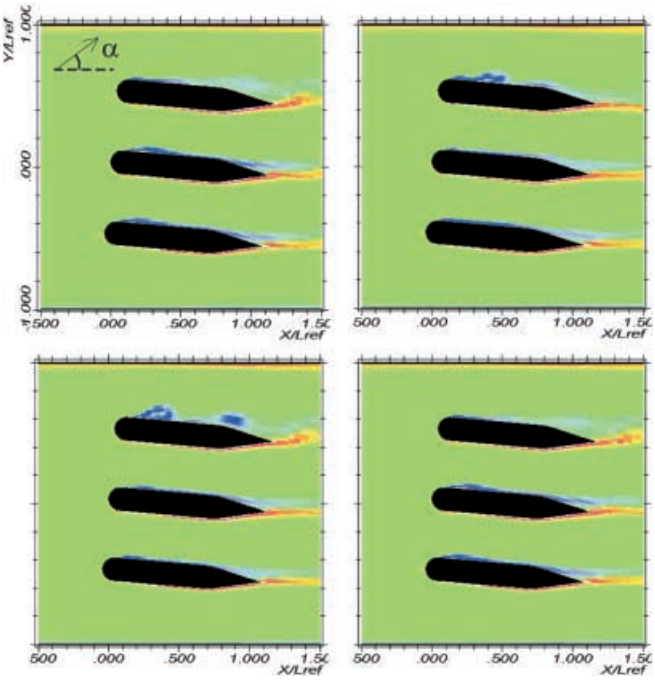

Fig. 11. Visualisation of the flow vorticity at t=143, 153, 164 and 174 ms

of the low-frequency cycle. The period of the low-frequency behaviour is then certainly linked to the convection time of the large vortices generated by unsteady cavitation, to the foil trailing edge.

Numerical calculations considering two other values of the cavitation number (σ=2.48 and σ=2.95) were also performed. Results concerning the auto-correlation functions obtained for high and low frequencies are illustrated in Fig. 12 for these two complementary cases. Characteristic frequencies can then be deduced and compared with the experimental ones (Fig. 2).

Numerical results present a good agreement with experimental values, and the code leads to a reliable simulation of the cyclic self-oscillation behaviour of unsteady cavitating flows.

6 Conclusion

Cavitation was studied in a cascade of three hydrofoils mounted in a cavitation tunnel. Estimation of the shedding and the coupling frequency was possible only in the auto-correlation domain due to the unsteadiness of the cycle duration and the low signal to noise ratio. Filter design on the basis of the frequency determination as described above is well suited for the extraction of interesting signal parts. Hilbert transformation and image phase averaging appeared to be a useful tool for getting detailed information about high-speed cyclic processes without the necessity of a high-speed camera.

Both the experimental and the numerical investigations show two dominant frequencies. The lower one is about 40 Hz in the experiments and does not depend on the cavitation number. It is found to be a little lower (30 Hz) by the numerical simulation. The higher fre-

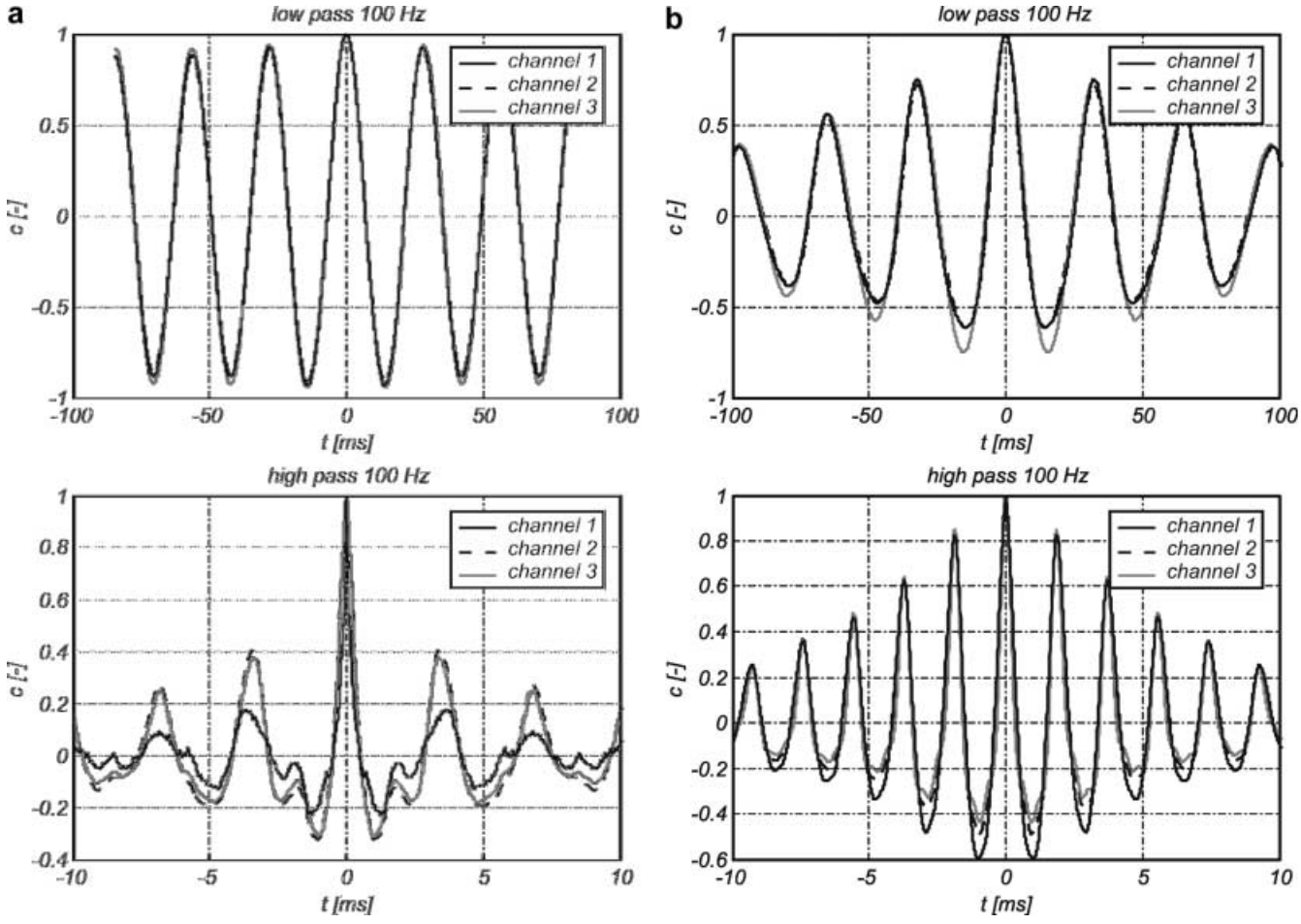

Fig. 12. **a** Auto-correlation functions obtained for high and low frequencies (σ=2.48). **b** Auto-correlation functions (σ=2.95)

quency corresponds to a Strouhal number close to 0.3 for the upper channel, where typical self-oscillating cloud cavitation is observed. At phase angles (for σ=1.95), when the cavitation in the upper channel is long, the cavitation structures in the other channels are short and vice versa.

According to the phase-averaged videos and the computation results, the lowest frequency seems to be strongly linked to the coupling of the three channels. Analyses of numerical results indicate that vortices generated by the cloud cavitation phenomenon in the upper channel are convected by the mean flow to the trailing edge. The flow repartition in the different channels seems to be strongly affected by the interaction between the travelling vortices and the trailing edge flow of the upper foil, which may be the origin of the low-frequency phenomenon.

The good agreement obtained between experimental and numerical results indicates that the proposed model well describes the unsteady cavitation behaviour and complex associated hydrodynamic effects.

References

Coutier-Delgosha O, Reboud JL, Albano G (2000) Numerical simulation of the unsteady cavitation behavior of an inducer blade cascade. Proceedings of 2000 ASME Fluid Engineering Summer Meeting, Cavitation and Multiphase Flow Forum, Boston, USA, June. ASME, New York

Coutier-Delgosha O, Fortes-Patella, R, Reboud JL (2001) Evaluation of the turbulence model influence on the numerical simulations of unsteady cavitation. Proceedings of 2001 ASME Fluid Engineering Summer Meeting, Cavitation and Multiphase Flow Forum, New Orleans, USA, June. ASME, New York

Delannoy Y, Kueny JL (1990) Two phase flow approach in unsteady cavitation modelling. Cavitation and Multiphase Flow Forum, ASME-FED 98:153–158

Hofmann M, Lohrberg H, Ludwig G, Stoffel B, Reboud JL, Fortes-Patella R (1999) Numerical and experimental investigations on the self-oscillating behavior of cloud cavitation. Part 1. Visualisation. Part 2. Dynamic pressures. Paper presented at the 3rd ASME/JSME Joint Fluids Engineering Conference, San Francisco, July

Hofmann M, Stoffel B, Coutier-Delgosha O, Fortes-Patella R, Reboud JL (2001) Experimental and numerical studies on a centrifugal pump with 2d-curved blades in cavitating condition. Paper presented at the 4th International Symposium on Cavitation, Pasadena

Joussellin F, Courtot Y, Coutier-Delgosha O, Reboud JL (2001) Cavitating inducer instabilities: experimental analysis and 2D numerical simulation of unsteady flow in blade cascade. Paper presented at the 4th International Symposium on Cavitation, Pasadena

Kubota A, Kato H, Yamaguchi H (1992) A new modelling of cavitating flows: a numerical study of unsteady cavitation on a hydrofoil section. J Fluid Mech 240:59–96

Reboud JL, Delannoy Y (1994) Two-phase flow modelling of unsteady cavitation. Paper presented at the 2nd International Symposium on Cavitation, Tokyo, April

Reboud JL, Stutz B and Coutier O (1998) Two-phase flow structure of cavitation: experiment and modelling of unsteady effects. Paper presented at the 3rd International Symposium on Cavitation, Grenoble, France, April

Sauer J, Schnerr GH (2000) Unsteady cavitating flow – A new cavitation model based on modified front capturing method and bubble dynamics. Proceedings of 2000 ASME Fluids Engineering Division Summer Meeting, Cavitation and Multiphase Flow Forum, Boston, USA, June. ASME, New York

Song CCS, He J (1998) Numerical simulation of cavitating flows by single-phase flow approach. Paper presented at the 3rd International Symposium on Cavitation, Grenoble, France, April

Zhu J (1991) A low diffusive and oscillation-free convection scheme. Commun Appl Num Methods 7:225–232